

Humanoid fall avoidance from random disturbances predicted via a Decision Volume

Noel El Khazen¹ Daniel Asmar¹ Najib Metni² and Elie Shammas¹

Abstract—Humanoid fall avoidance is the ability of a robot to avoid falling when pushed. The decision surface is a region on the phase diagram delimiting the states beyond which the robot cannot recover from a disturbance. The disadvantage of the decision surface is that it is limited to perturbations in the sagittal and coronal planes. This paper deals with the generalization of the decision surface to a *decision volume*, used for the prediction of limiting states for recovery from disturbances in any orientation. A second contribution is the extension of the ankle strategy for humanoid fall avoidance to disturbances in random directions. The model used is a 3D Linear Inverted Pendulum Model (LIPM). Both, ankle strategy and decision volume are tested on the Webots simulator then implemented on a real humanoid robot.

I. INTRODUCTION

Although the past decades have finally witnessed the introduction of robots into our homes, most of them—like the Roomba vacuum cleaner—are wheeled platforms. On the other hand, a humanoid robot is designed with kinematics emulating those of a human in order to negotiate environments originally conceived and designed to accommodate human motion. With this constraint in mind, humanoids should be endowed with the ability to avoid falling when pushed from different directions. Although keeping balance is trivial for humans it is in fact quite challenging to implement on humanoids, which are open-chained underactuated mechanisms.

According to Winter [1], [2], the Center of Mass (CoM) of humans is located at two-thirds of their height. In consequence, this makes humans inherently unstable systems, needing a control system that is continuously acting. Winter cites two strategies that are implemented by humans for fall avoidance. The first one is the ankle strategy, which is effective for a small disturbance, by counteracting it with a torque at the ankles. For larger perturbations, the hip strategy—using both ankle and hip joints to create a momentum by rotating the torso at the hips—is used. If the push is yet larger and both the ankle and hip reflexes are not sufficient, then the human is forced to take one or several steps in order not to fall.

Stephens [3] originally developed the decision surface for the ankle strategy, then followed by Jalgha *et al.* [4],

[5] and Asmar *et al.* [6] for the hip strategy. Having the initial states (position and velocity) of the robot, the decision surface determines whether the robot is able to recover from a push, and which strategy is appropriate to use. Jalgha *et al.* also implemented the strategies on a humanoid using Virtual Model Control (VMC) [7]. One disadvantage of the decision surface is that it is limited to disturbances in the coronal or sagittal planes.

The capture point is another method developed by Pratt *et al.* [8], [9], [10], [11], and it represents a point on the ground where the robot can step to in order to bring itself to a complete stop. Depending on the capture point location, a robot may use its ankles, hips, or even take one or several steps to recover. Goswami *et al.* [12] used the machine learning approach to predict falls. These methods do not have a defined boundary that is used to determine their effectiveness.

In light of the limitations in the literature, this paper introduces a technique for recovery from disturbances in random directions. As an initial step we develop our technique for the ankle strategy, and implement it to a simulated as well as a real robot. Furthermore, we present what we call the *decision volume*—extending the idea of the decision surface—to draw the limiting state conditions on a 3D plot. What will be observed is that the decision volume is solely determined by the robot's geometry and mass but not a function of time. Given the robot's initial velocity and position, the stability of our system can now be evaluated in the more general case of random disturbances.

The remainder of this paper is structured as follows. Section II covers a brief background on fall avoidance using the ankle strategy. Section III puts forward the model that is used for the humanoid for motion in 2D. Section IV develops the decision volume upon which our system is based. Section V discusses the control strategy for fall avoidance in 2D. Section VI presents the experiments and corresponding results of the fall avoidance scheme applied on our simulated humanoid as well as on a real humanoid robot. Finally Section VII concludes the paper and indicates the direction of our future work.

II. ANKLE STRATEGY IN 1D

A bipedal robot is inherently unstable by nature. In its simplest form, we consider that all the humanoid's limbs and joints situated above the ankle joint are stiff and model the humanoid as an inverted pendulum pinned to the ground via its ankle joint. This model is valid as long as the foot is flat over the ground and the ankle joint can be controlled

*This work was partly supported by a grant from the University Research Board (URB) at the American University of Beirut and partly by the Lebanese National Council for Scientific Research (LNCSR)

¹ Noel El Khazen, Daniel Asmar, and Elie Shammas are with the Department of Mechanical Engineering, American university of Beirut, Lebanon nse14@aub.edu.lb, da20@aub.edu.lb, es34@aub.edu.lb,

² Najib Metni is with the Department of Mechanical Engineering, Notre Dame University, Zouk, Lebanon nmetni@ndu.edu.lb

as one would control a joint of a robotic arm. However, a humanoid is constrained by a limited foot-ground interaction [13]. As soon as the robot becomes unstable, the foot starts rotating, the robot loses controllability of the ankle joint, and the robot eventually falls down.

The stability problem of a humanoid robot consists of looking into ways in which to keep the states controllable, or even look into ways that would bring the robot back into a controllable space. This requires the use of strategies such as the ankle strategy, the momentum strategy, and the stepping strategy. In the ankle strategy a human compensates for a disturbance just like an inverted pendulum does, simply by providing an ankle torque that counteracts the disturbance and prevents the fall. Due to the limited foot ground interaction, the ankle torque is limited and can only be used as a preventive falling measure in the case of small disturbances.

The inverted pendulum model of a biped (Fig. 1) was first pointed out by Hemami et al. [14]. The body as a whole is treated as a point mass located at the center of mass (CoM) and only the muscle dynamics at the ankle joint are involved.

Deciding when to apply which fall avoidance strategy is based on a model that is developed for each strategy, which is capable of inferring from the current state (*e.g.*, angular position and angular velocity) of the humanoid if it can recover by applying the corresponding strategy. Stephens [3] was the first to introduce what is known as decision surfaces for humanoid push recovery strategies. A decision surface delineates the thresholds (or 2D region if we consider a 2 DoF robot) beyond which the robot cannot avoid falling by applying the corresponding fall avoidance strategy. The procedure to determine the decision surface is to first consider a disturbance that drives the system to the border of stability. At this state the CoP reaches the edge of the foot and $T_a = -mg\delta$, where δ is the distance from the ankle joint to the edge of the foot (Fig. 1a). The initial values of θ and $\dot{\theta}$ for which the CoP reaches the edge of the foot delineate the borders of our decision surface. Jalgha *et al.* [5] found this region to be specified as:

$$f^- < \theta_0 + \frac{\dot{\theta}_0}{\omega} < f^+, \quad (1)$$

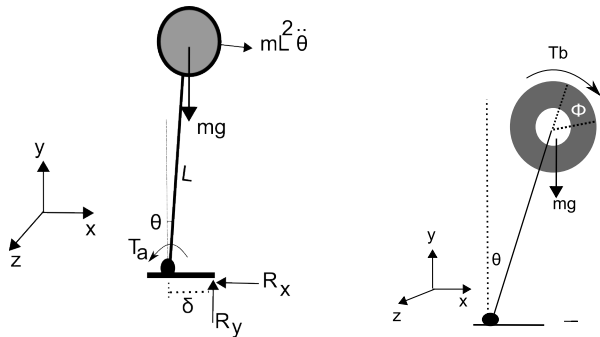


Fig. 1: The inverted pendulum model (left) and the angular momentum pendulum model (right).

where $f^\pm = \delta^\pm/L$ and $\omega = \sqrt{g/z_c}$. Anytime θ and $\dot{\theta}$ of the system get beyond this decision surface area the ankle strategy is no longer capable of preventing the robot from falling and an alternate solution such as a momentum strategy is required.

Moving from a 1D to a 2D disturbance requires modeling the motion of the robot in a 3D, and also to develop a delimiting region in 3D—which we call decision volume.

III. DYNAMIC MODEL IN 3D

Several authors have suggested methods for Modeling and controlling humanoid robots in 3D. Kajita *et al.* [15], [16] introduced the 3D Linear Inverted Pendulum Model (3D-LIPM) to generate walking patterns for humanoids. This pendulum (Fig.2) can rotate around both the x-axis and the y-axis. It possesses a prismatic joint that adds a degree of freedom for accounting for the robot's mass. To simplify this model, the CoM is considered to move along an arbitrary defined plane, which is described by its normal vector $\vec{n}(a, b, -1)$ and intersects the z-axis at z_c . The equation of the this plane is expressed as

$$z = ax + by + z_c \quad (2)$$

In our model, the robot's CoM is assumed to be constrained to move at a constant height $z = z_c$ and the normal vector \vec{n} subsequently reduces to $(0, 0, -1)$.

Restricting mass movement to a horizontal plane linearizes the equations of motion developed in [17] and results in the following equations

$$\ddot{x} = \frac{g}{z_c}x + \frac{1}{mz_c}\tau_y, \quad (3)$$

$$\ddot{y} = \frac{g}{z_c}y - \frac{1}{mz_c}\tau_x, \quad (4)$$

where g represents gravitational acceleration, m the pendulum's mass and τ_x, τ_y the torques across the x-axis and the y-axis respectively.

IV. DECISION VOLUME

In order to better understand stability for humanoid robots the concepts of Center of Pressure (CoP) and Zero Moment point (ZMP) are introduced. CoP is defined as the location

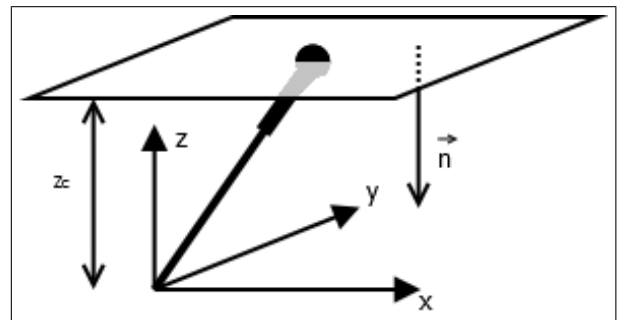


Fig. 2: 3D Linear Inverted Pendulum limited to a horizontal plane.

where an equivalent ground reaction force under the foot's support is represented. ZMP [18] on the other hand is the location on the ground where the robot's inertial, gravitational, Coriolis, and centrifugal forces are balanced by the reaction force. The concepts of COP and ZMP are used together in order to establish the stability of a humanoid. If the ZMP is inside the foot soles, the COP has to follow the ZMP in order for the system to be brought back to equilibrium. If the ZMP position exceeds the foot sole, the robot should take action (such as the momentum strategy or take a step) in order to bring the ZMP back inside the region where a reaction force at the CoP keeps the humanoid from falling down.

In a biped system, all joints are powered and directly controlled except the contact between the foot and the ground, which can be considered as a passive joint [19]. Although this virtual joint cannot be directly controlled, it is affected by the dynamics of the mechanisms above the foot, which can change the location of the ZMP and thus create a torque on the passive joint. Equations (5) and (6) present the relation between the position of the ZMP and its equivalent torques. The further away the ZMP is located, the greater the value of its torque.

$$p_x = \frac{-\tau_y}{m.g}, \quad (5)$$

$$p_y = \frac{\tau_x}{m.g}. \quad (6)$$

Where the ZMP position is limited to the support polygon of the robot it coincides with the CoP. If the ZMP position exceeds the foot sole it is called the fictitious ZMP (FZMP) [18]. In that case, the CoP remains at the edge of the sole and the difference between the FZMP and the CoP creates a tipping moment. To proceed with the development of the decision volume, (5) and (6) are rearranged for expressions in τ_y and τ_x , which are then substituted into (3) and (4)

$$\ddot{x} = \frac{g}{z_c}(x - p_x), \quad (7)$$

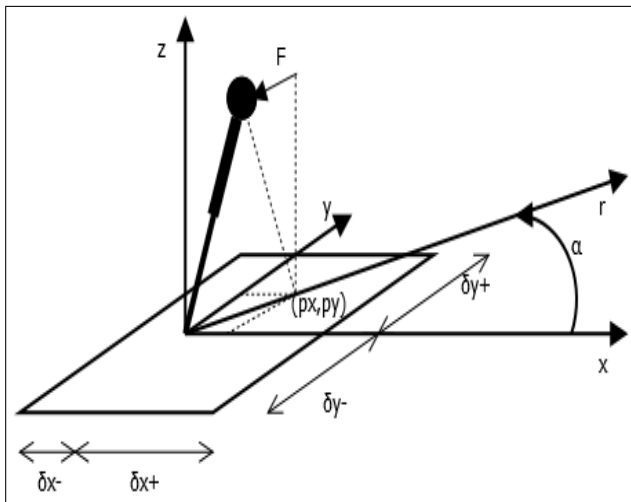


Fig. 3: ZMP for the 3D-LIPM.

$$\ddot{y} = \frac{g}{z_c}(y - p_y). \quad (8)$$

By substituting $x = r \cos \alpha$, $y = r \sin \alpha$, $p_x = p_r \cos \alpha$ and $p_y = p_r \sin \alpha$ into (7) and (8) and taking the sum of their squares results in

$$\ddot{r} = \frac{g}{z_c}(r - p_r), \quad (9)$$

The angle α determines the line of action shown in Fig. 3 as the r -axis. The value of α is independent of time and is determined based on the direction of the push and the initial velocity vector (\dot{r}_0). To cover all points in the xy -plane, $\alpha \in [-\frac{\pi}{2}; \frac{\pi}{2}]$ and $r \in]-\infty; \infty[$.

When a robot is pushed, it is given an initial velocity \dot{r}_0 along the r -axis. To decelerate, the difference between the CoM (r) and ZMP (p_r) must be negative. Fig. 3 shows how the ZMP affects the pendulum. The torque generated by the ZMP is replaced by its equivalent force F . Since the location of the ZMP is limited to the support polygon, the equivalent recovery force F is also limited. This constraint is the basis for the limits imposed by the decision volume. Solving (9) results in

$$r(t) = \frac{1}{2}(r_0 + \frac{\dot{r}_0}{\omega} - p_r)e^{\omega t} + \frac{1}{2}(r_0 - \frac{\dot{r}_0}{\omega} - p_r)e^{-\omega t} + p_r, \quad (10)$$

where r_0 and \dot{r}_0 represents the initial position and velocity respectively.

For the system to be stable, the coefficient of $e^{\omega t}$ in (10) must be zero. So the stability condition becomes,

$$\delta_r^- < r_0 + \frac{\dot{r}_0}{\omega} < \delta_r^+ \quad (11)$$

where δ_r^+ and δ_r^- represent the upper and lower bound for the ZMP across the r -axis, respectively. This inequality is valid for each angle α . To find the ZMP bounds the intersections between the vector r and the support polygon are calculated based on the value of α . Three regions are identified for positive values of δ_r and three for negative values.

$$\delta_r^+ = \begin{cases} \frac{\delta_y^-}{\sin \alpha} & \alpha \in [-\pi/2, \text{atan2}(\delta_y^-, \delta_x^+)] \\ \frac{\delta_x^+}{\cos \alpha} & \alpha \in [\text{atan2}(\delta_y^-, \delta_x^+), \text{atan2}(\delta_y^+, \delta_x^+)] \\ \frac{\delta_y^+}{\sin \alpha} & \alpha \in [\text{atan2}(\delta_y^+, \delta_x^+), \pi/2] \end{cases} \quad (12)$$

$$\delta_r^- = \begin{cases} \frac{\delta_y^+}{\sin \alpha} & \alpha \in [-\pi/2, \text{atan2}(\delta_y^+, \delta_x^-) - \pi] \\ \frac{\delta_x^-}{\cos \alpha} & \alpha \in [\text{atan2}(\delta_y^+, \delta_x^-) - \pi, \text{atan2}(\delta_y^-, \delta_x^-) + \pi] \\ \frac{\delta_y^-}{\sin \alpha} & \alpha \in [\text{atan2}(\delta_y^-, \delta_x^-) + \pi, \pi/2] \end{cases} \quad (13)$$

where δ_x and δ_y represent the dimensions of the support polygon of the robot. Fig. 4 shows the decision volume for a NAO robot (used in our experiments) with $z_c = 0.3$ m, $\delta_x^+ = 0.105$ m, $\delta_x^- = -0.046$ m, $\delta_y^+ = 0.105$ m, and $\delta_y^- = -0.105$ m.

An additional limit is added to the decision volume due to a geometric constraint. In fact, the maximum position the CoM position can reach is $r = z_c$, because it is physically limited in length. As a result the decision volume will be reduced to the region shown in Fig 4. This volume shows

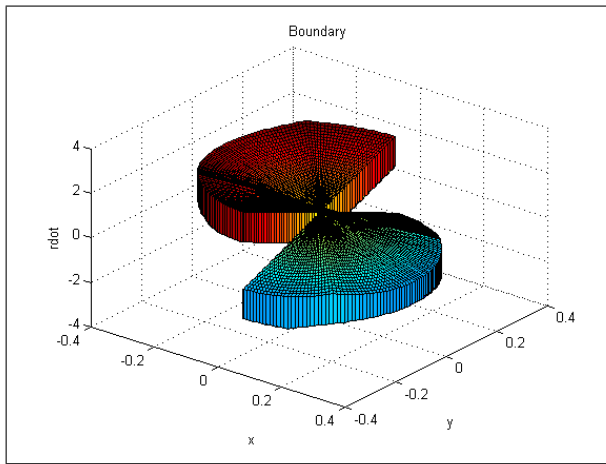


Fig. 4: Decision volume for ankle strategy.

the three states of the robot $(x_{CoM}, y_{CoM}, \dot{r})$ where the ankle strategy would be successful in returning the humanoid to its equilibrium position.

V. CONTROL

To control our system we use the Virtual Model Control VMC, which consists of using virtual mechanical components such as springs and dampers in order to compute the forces and moments required to actuate a robots motors. For the model in this paper one spring and one damper are attached to the CoM along each of the x -axis and the y -axis. The resultant forces of the virtual springs and dampers are

$$F_x = -K_x x - B_x \dot{x}, \quad (14)$$

$$F_y = -K_y y - B_y \dot{y}. \quad (15)$$

Since these components are virtual, their desired effect is applied to the robot via the ankles roll and pitch motor torques.

$$\tau_x = F_y z_c + mgy \quad (16)$$

$$\tau_y = F_x z_c - mgx \quad (17)$$

Fig. 5 shows the trajectory of the CoM mapped onto a contour plot section of the decision volume corresponding to given velocity magnitude (\dot{r}). As long as the CoM remains within this contour plot, the humanoid system can be brought back to its equilibrium state. In this simulation, the initial velocity \dot{r} is equal to $0.5m/s$, the angle α is $\pi/4$, and control parameters are $K_x = K_y = 50$ and $B_x = B_y = 35$. Through this simulation angle α remains constant, which is consistent with our previous statement, and the CoM follows a straight line. Referring to Fig. 5, when the velocity of the robot is relatively high (top sub-figure, $t = 0s$) the region of maneuverability of the robot is relatively small. As the robot slows down (middle sub-figure, $t = 0.0886s$) it is less constrained and has a larger z_c to maneuver within. Finally, once the speed is equal to zero (bottom sub-figure) the cross section of the decision volume becomes equal to the support polygon of the robot.

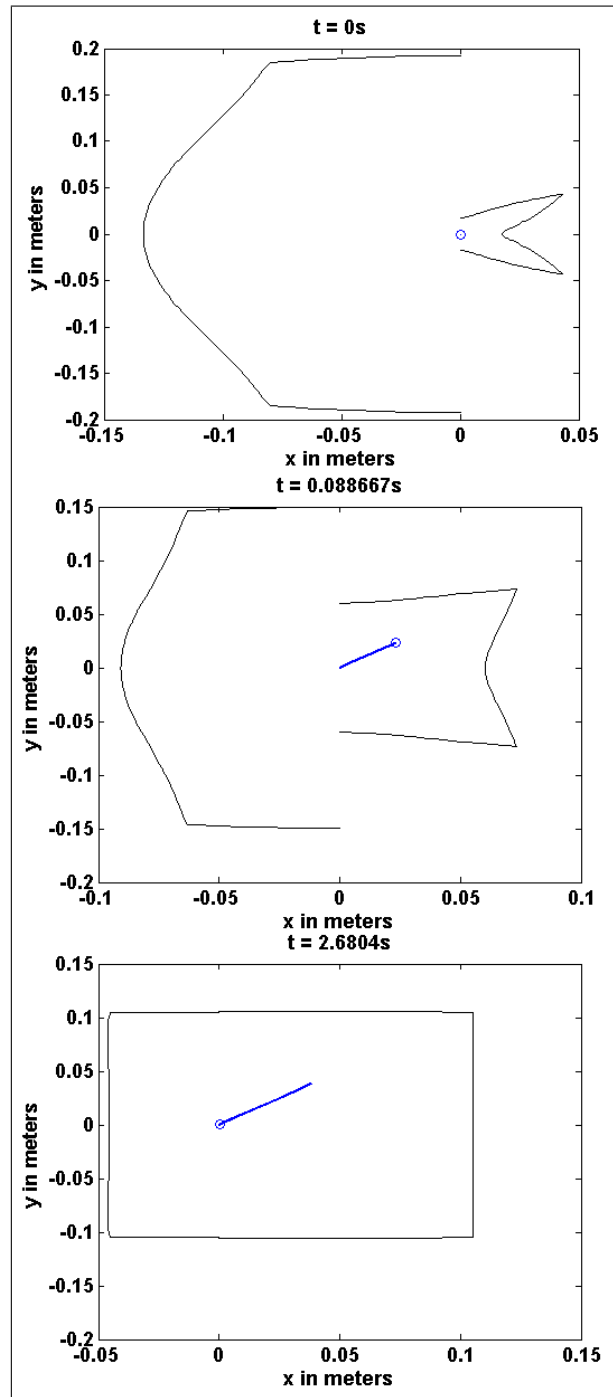


Fig. 5: 3D-LIPM simulation $\dot{r}_0 = 0.5m/s$ and $\alpha = \pi/4$.

In practice, the robot has four motors at the ankles that need to be actuated—for each foot one for the pitch and another for the roll. Force sensors below each foot feedback to the system the current state of the reaction forces on the ground and weights are assigned based on the distribution of these forces. The motors are actuated in one of two modes. In the first mode (Fig. 6, left) both feet of the robot are on the ground, and the motors are actuated according to the weights determined above. In the second mode (Fig. 6) only one foot is in contact with the ground and it is solely responsible for

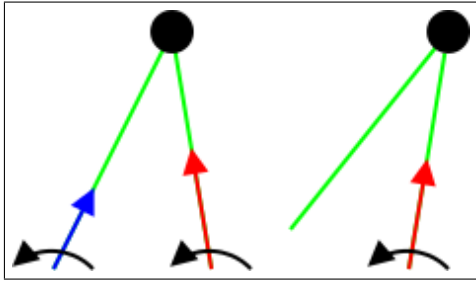


Fig. 6: Torque distribution on ankles motors.

supplying the torque required by the VMC.

VI. EXPERIMENTS AND RESULTS

To prove the validity of our proposed all-directional fall avoidance system several experiment are performed on a simulated as well as a real robot. The NAO humanoid robot [20] is used for both the simulations—implemented on Webots [21], [22]—as well as the live robot tests. NAO is a 58cm humanoid that features 25 degrees of freedom. It is equipped with a large array of sensors including encoders, an IMU (inertial measurement unit), cameras, and force sensors under the feet. Although the robot does not support torque control, the allowable torque can be fixed in order to emulate it.

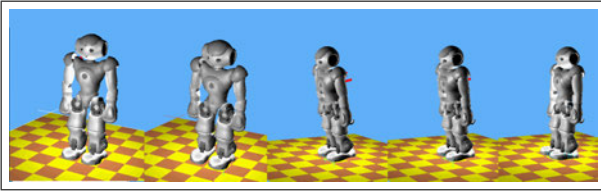


Fig. 7: Webots simulation (25 N of force at an angle of $\pi/4$).

Fig. 7 shows snapshots of a Webots simulation, where the amplitude of the force is 25 N imparted at an angle of $\pi/4$. The force was applied at a height of 0.4 m from the ground with a duration of 0.1 sec. In Fig. 8 the CoM trajectory traced for the same disturbance as in Fig.7 and reaches a maximum of 0.033 m in the x direction, and 0.017 m in the y direction. The trajectory is not a straight line as in Fig. 5. When the robot is pushed, the CoM starts moving along a straight line. Reaching the edge, the foot has partially lost its contact with the ground and this causes a small modification in the trajectory. Fig. 9 show the variation of \dot{r} in function of time. The figure shows how when the robot is pushed the velocity \dot{r} increases to a maximum value of 0.28 m/s and then the ankle strategy decelerates the robot and returns it to an equilibrium state—albeit with some oscillations. Fig. 10 shows the decision volume, where x , y and \dot{r} are plotted. The decision volume agrees with the fact that the robot can recover from the applied disturbance since the states do not exit the decision volume at any point in time.

Finally in Fig. 11 the ankle strategy is implemented on the real NAO humanoid. The robot is struck by a ball, which imparts a disturbance force of 46.5 N as measured by a force

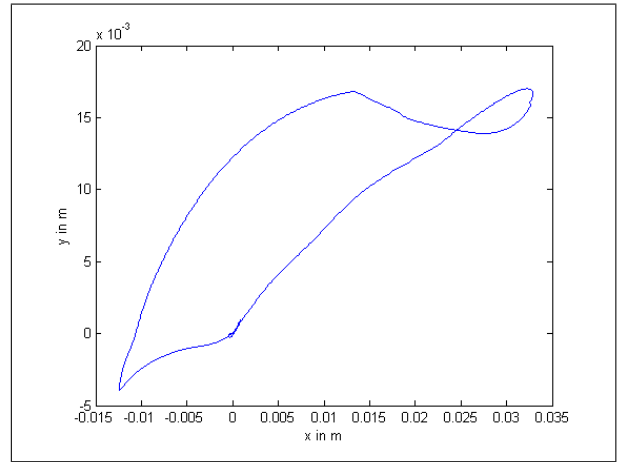


Fig. 8: CoM trajectory for simulated NAO struck by 25 N force for 0.1 sec.

sensor. By examining these snapshots closely, the robot’s left foot partially loses contact with the ground, at which time it applies the second mode of recovery mentioned in Section V. When the robot is pushed by the ball, the CoM moves 0.056 m to the front and 0.02 m to the right as shown in Fig. 12 and Fig. 13 respectively. These values are consistent with the ball direction, since the ball is coming from the back left side.

VII. CONCLUSIONS AND FUTURE WORK

To conclude, the decision volume was successful in determining at which states the ankle strategy is sufficient to recover from a sudden disturbance while standing still. Also, the robot has no prior knowledge of the amplitudes and directions of the push. Both of the ankles are actuated in the roll and pitch directions. The robot is capable each time to restore its balance and return to its initial equilibrium position.

The next step will be to develop a decision volume for the hip strategy, where hips are used to rotate robot’s torso and create a torque to restore balance. Using this additional strategy the humanoid should be capable of recovering from

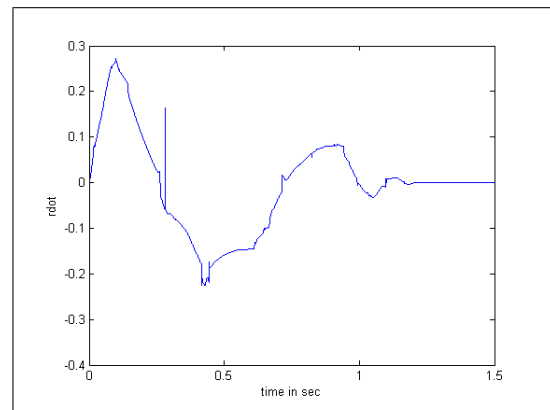


Fig. 9: \dot{r} in function of time.

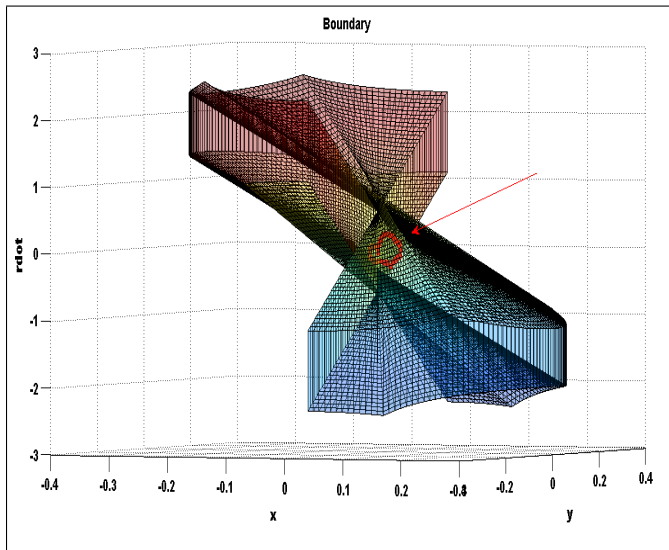


Fig. 10: Decision volume for Webots simulation, arrow indicates robot state evolution throughout recovery.

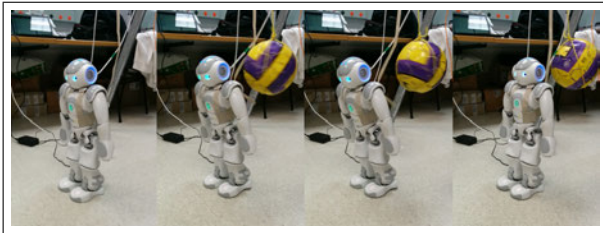


Fig. 11: Ankle strategy applied to real robot.

larger disturbances. However, since hips cannot accelerate indefinitely, this also creates constraints delimiting an augmented decision volume.

REFERENCES

- [1] D. A. Winter, "Human balance and posture control during standing and walking," *Gait & posture*, vol. 3, no. 4, pp. 193–214, 1995.
- [2] D. A. Winter, A. E. Patla, S. Rietdyk, and M. G. Ishac, "Ankle muscle stiffness in the control of balance during quiet standing," *Journal of Neurophysiology*, vol. 85, no. 6, pp. 2630–2633, 2001.
- [3] B. Stephens, "Humanoid push recovery," *Proceedings of the IEEE/RSJ conference on Intelligent Robots and Systems*, 2007.
- [4] B. Jalgha and D. C. Asmar, "A simple momentum controller for humanoid push recovery," in *Advances in Robotics*, pp. 95–102, Springer, 2009.
- [5] B. Jalgha, D. Asmar, and I. Elhajj, "A hybrid ankle/hip preemptive falling scheme for humanoid robots," in *Robotics and Automation (ICRA), 2011 IEEE International Conference on*, pp. 1256–1262, IEEE, 2011.
- [6] D. C. Asmar, B. Jalgha, and A. Fakh, "Humanoid fall avoidance using a mixture of strategies," *International Journal of Humanoid Robotics*, vol. 9, no. 01, 2012.
- [7] J. Pratt, C.-M. Chew, A. Torres, P. Dilworth, and G. Pratt, "Virtual model control: An intuitive approach for bipedal locomotion," *The International Journal of Robotics Research*, vol. 20, no. 2, pp. 129–143, 2001.
- [8] J. Pratt, J. Carff, S. Drakunov, and A. Goswami, "Capture point: A step toward humanoid push recovery," in *Humanoid Robots, 2006 6th IEEE-RAS International Conference on*, pp. 200–207, IEEE, 2006.
- [9] T. Koolen, T. De Boer, J. Rebula, A. Goswami, and J. Pratt, "Capturability-based analysis and control of legged locomotion, part 1: Theory and application to three simple gait models," *The International Journal of Robotics Research*, vol. 31, no. 9, pp. 1094–1113, 2012.

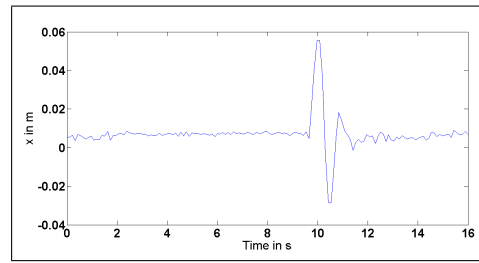


Fig. 12: x_{CoM} in function of time.

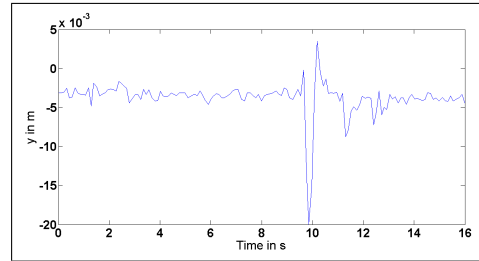


Fig. 13: y_{CoM} in function of time.

- [10] J. Pratt, T. Koolen, T. De Boer, J. Rebula, S. Cotton, J. Carff, M. Johnson, and P. Neuhaus, "Capturability-based analysis and control of legged locomotion, part 2: Application to m2v2, a lower-body humanoid," *The International Journal of Robotics Research*, vol. 31, no. 10, pp. 1117–1133, 2012.
- [11] J. E. Pratt and S. V. Drakunov, "Derivation and application of a conserved orbital energy for the inverted pendulum bipedal walking model," in *ICRA*, pp. 4653–4660, 2007.
- [12] S. Kalyanakrishnan and A. Goswami, "Learning to predict humanoid fall," *International Journal of Humanoid Robotics*, vol. 8, no. 02, pp. 245–273, 2011.
- [13] J. E. Pratt, *Exploiting Inherent Robustness and Natural Dynamics in the Control of Bipedal Walking Robots*. Massachusetts Institute of Technology: PhD thesis, May 2000.
- [14] H. Hemami, C. Wall, F. Black, and G. Golliday, "Single inverted pendulum biped experiments," *Journal of Interdisc. Model. and Simul.*, vol. 2, no. 3, 1979.
- [15] S. Kajita, F. Kanehiro, K. Kaneko, K. Yokoi, and H. Hirukawa, "The 3d linear inverted pendulum mode: A simple modeling for a biped walking pattern generation," in *Intelligent Robots and Systems, 2001. Proceedings. 2001 IEEE/RSJ International Conference on*, vol. 1, pp. 239–246, IEEE, 2001.
- [16] S. Kajita, F. Kanehiro, K. Kaneko, K. Fujiwara, K. Harada, K. Yokoi, and H. Hirukawa, "Biped walking pattern generation by using preview control of zero-moment point," in *Robotics and Automation, 2003. Proceedings. ICRA'03. IEEE International Conference on*, vol. 2, pp. 1620–1626, IEEE, 2003.
- [17] S. Kajita, O. Matsumoto, and M. Saigo, "Real-time 3d walking pattern generation for a biped robot with telescopic legs," in *Robotics and Automation (ICRA), IEEE International Conference on*, no. 2299–2308, 2001.
- [18] M. Vukobratovic and B. Borovac, "Zero-moment point, thirty five years of its life," *International Journal of Humanoid Robotics*, vol. 18, pp. 157–173, 2007.
- [19] M. Vukobratović and B. Borovac, "Zero-moment point—thirty five years of its life," *International Journal of Humanoid Robotics*, vol. 1, no. 01, pp. 157–173, 2004.
- [20] Aldebaran-Robotics, "http://www.aldebaran-robotics.com/en/." French Robotics Company.
- [21] webots, "http://www.cyberbotics.com." Commercial Mobile Robot Simulation Software.
- [22] O. Michel, "Webots: Professional mobile robot simulation," *Journal of Advanced Robotics Systems*, vol. 1, no. 1, pp. 39–42, 2004.